Imaging of the Hydrogen Subsurface Site in Rutile TiO_2

Georg H. Enevoldsen,[1] Henry P. Pinto,[2] Adam S. Foster,[2,3,*] Mona C. R. Jensen,[1] Werner A. Hofer,[4] Bjørk Hammer,[1] Jeppe V. Lauritsen,[1] and Flemming Besenbacher[1,†]

[1]*Interdisciplinary Nanoscience Center (iNANO) and Department of Physics and Astronomy, University of Aarhus, Denmark*
[2]*Laboratory of Physics, Helsinki University of Technology, P.O. Box 1100, FI-02015 TKK, Finland*
[3]*Department of Physics, Tampere University of Technology, P.O. Box 692, 33101, Finland*
[4]*Surface Science Research Centre, The University of Liverpool, Liverpool, United Kingdom*

(Received 27 November 2008; published 1 April 2009)

From an interplay between simultaneously recorded noncontact atomic force microscopy and scanning tunneling microscopy images and simulations based on density functional theory, we reveal the location of single hydrogen species in the surface and subsurface layers of rutile TiO_2. Subsurface hydrogen atoms (H_{sub}) are found to reside in a stable interstitial site as subsurface OH groups detectable in scanning tunneling microscopy as a characteristic electronic state but imperceptible to atomic force microscopy. The combined atomic force microscopy, scanning tunneling microscopy, and density functional theory study demonstrates a general scheme to reveal near surface defects and interstitials in poorly conducting materials.

DOI: 10.1103/PhysRevLett.102.136103 PACS numbers: 68.47.Gh, 61.72.jj, 68.37.Ef, 68.37.Ps

Atomic defects may have an overriding effect on physical and chemical properties of materials, and many technologies rely on detailed control of atomic impurities, promoters, or dopants, such as in semiconductors, gate oxides, optics, or (photo)catalysts. In catalysis, the importance of surface defects and atomic vacancies has long been established [1], whereas the subsurface region has traditionally not been considered to be very important. However, subsurface oxygen vacancies observed on $CeO_2(111)$ have been proposed to play a key role in the oxygen release process [2] vital to its catalytic properties in oxidation reactions [3]. Also, studies have shown that ubiquitous Ti interstitials are responsible for donor levels in TiO_2 [4], which may be important for the photocatalytic properties. Additionally, hydrogen is a predominant and important impurity in the bulk of semiconductors and metal oxides [5,6]. The hydrogen may change the material properties by acting as a dopant or by quenching defect states and thereby modify charge carrier lifetimes important for photocatalytic or photoluminescence applications. However, analytical methods which can reveal atomic defects below the topmost layer, such as H or O vacancies, are currently not well developed. Here we demonstrate how simultaneously recorded noncontact atomic force microscopy (nc-AFM) and scanning tunneling microscopy (STM) images in conjunction with density functional theory (DFT) based image simulation may be applied to unambiguously assign the site of single H atoms in the subsurface region of rutile $TiO_2(110)$. Whereas the AFM provides a map of the tip-surface force, the STM measures the tunneling current, which represents convolution of geometric structure and the local electronic structure. The sensitivity to atomic defects may therefore be distinctly different in AFM and STM due to a larger range of electronic states pinned at defects. When applied simultaneously [7–9], the complementary information obtained from STM and AFM may be used in a unique way to deconvolute geometric and electronic effects and, as demonstrated here for a $TiO_2(110)$ model system, discriminate between two types of atomic H species in TiO_2—H in surface OH groups, which appear in both channels, and subsurface H atoms as OH_{sub} groups, which exclusively appear in the STM images as an electronic perturbation. DFT total energy calculations and STM image simulations implementing the accurate nanoscale structure of the imaging tip verify the energetic stability and the characteristic STM I_t signature of both sOH and OH_{sub} species.

The experiments were carried out at room temperature and under UHV conditions on a prehydroxylated $(1 \times 1)TiO_2(110)$ surface [10,11]. Simultaneous STM and AFM imaging was performed by operating the nc-AFM in the topography mode where the AFM frequency shift (Δf) is used as feedback signal [12] while simultaneously recording the oscillation averaged tunneling current between the tip and surface atoms as a passive signal in an additional channel. The bias voltage applied to the tip U_{bias} was adjusted to minimize the electrostatic forces. For further experimental details, we refer the reader to Refs. [8,10].

DFT calculations were performed using the VASP code [13] employing projected augmented wave potentials [14] (including Ti-3s and -4p semicore states) and the spin-polarized local density approximation plus on-site repulsion (LDA + U) method. Our results show that for defective $TiO_2(110)$ LDA + U, including on-site Coulomb interaction between Ti-3d electrons [15], performs better than Perdew-Burke-Erhnzoff in terms of density localization and calculated current [16]. We reproduced the ex-

perimental TiO_2 bulk structure [11] with a Dudarev parameter of $\mathcal{U} = 3.6$ eV that produces a ~2.2 eV band gap [17]. The TiO_2(110) surface was modeled by a 2×4 slab with five O-TiO_2-O "trilayers" (freezing the lowest two trilayers during relaxations) and 15 Å vacuum along the [110] direction (further details of the testing of this setup are given in Ref. [8]). Using a cutoff energy of 450 eV and a Γ centered $2 \times 2 \times 1$ Monkhorst-Pack k-point mesh, we converge the total energy to <1 meV/atom. Finally, all of the structures were fully relaxed until all of the forces were <0.01 eV/Å, and the climbing nudged elastic band method [18] was used to identify the reaction energy path. Simulated STM images were performed using multiple electron scattering with a Green's function formalism implemented in the BSKAN code [8,19]. For direct comparison of the simulations with the experiment, we used the measured AFM tip trajectory to calculate the resulting tunneling current [8].

We have recently presented detailed nc-AFM studies of the TiO_2(110) surface, identifying all atoms in the topmost surface layer including single oxygen vacancies and surface hydroxyls (sOH) based on their appearance in nc-AFM images [10]. It was clearly demonstrated how the Ti or O sublattices, and the surface defects, appear in three distinctly different nc-AFM contrast modes explained by the contribution depending on the polarity of the localized chemical force between the surface and a tip terminated by either an electropositive (O-terminated), electronegative (Ti-terminated), or neutral nanoapex (Si), respectively. In Fig. 1(a), a nc-AFM image of the TiO_2(110) surface is presented, which was recorded with a negatively terminated tip. Here we can identify the fivefold coordinated in-plane titanium atoms [Ti(5c), nominal charge +4] as the bright rows (maximum attractive force). Conversely, the twofold coordinated bridging oxygen atoms [O(2c) with a nominal charge of −2] are imaged as dark rows (minimum attractive force), with several single bridging hydroxyls (sOH) visible as bright protrusions in between the bright Ti rows. Figure 1(b) shows the corresponding simultaneously recorded STM (I_t) image where the Ti are imaged as bright rows relative to the dark O rows. From comparison, the bridging sOH groups (circles) also appear with a similar bright STM contrast on the dark O rows. However, in addition, we can identify a different species (squares), appearing only in the STM image as rather faint protrusions. Surprisingly, there is no indication of a defect-related signature in the AFM signal over these sites (squares), which suggests that the tip-surface force has been completely screened.

We can obtain further information on the apparent subsurface species by analyzing a time-resolved sequence of STM and AFM images. Figures 1(c) and 1(d) show simultaneously recorded nc-AFM and STM images recorded 4 min after Figs. 1(a) and 1(b). From comparison, it is evident that the surface does not reflect a static situation. Instead, we observe the dynamic conversion of two sOH

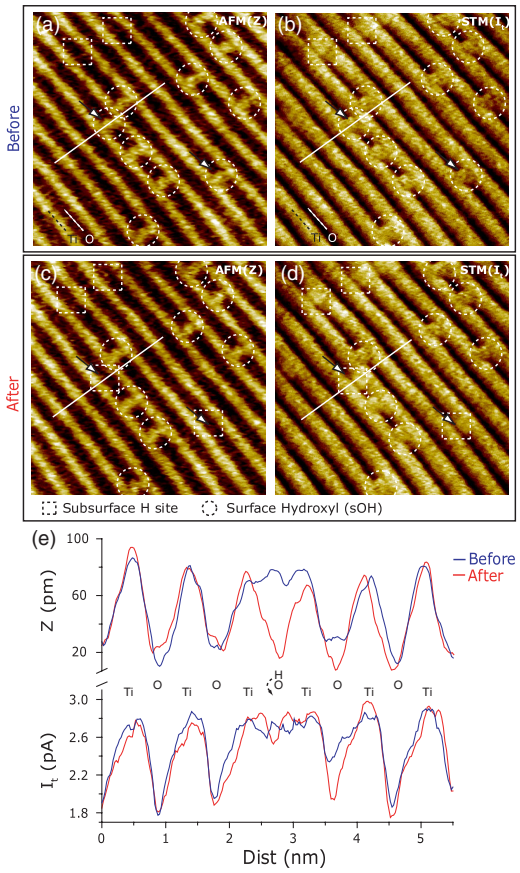

FIG. 1 (color online). (a),(c) nc-AFM topography images of the TiO_2(110) surface recorded with a time lapse of 4 min. Size $= 10 \times 10$ nm^2, $\Delta f = -46.9$ Hz, $U_{\text{bias}} = 0.97$ V, and $A_{p-p} \sim 25$ nm. (b),(d) Simultaneously recorded tunneling current (STM) images (I_t) of (a) and (c), respectively. Circles: Bridging OH; squares: subsurface OH. (e) Overlapped line scans showing the AFM and STM corrugation before (blue) and after (red) a H atom was moved to the subsurface site.

(circles with arrow) into two OH_{sub} (squares), which are again visible only in the STM images. Considering only the nc-AFM image, it may seem plausible to conclude that the H of the sOH has desorbed, e.g., by the scanning tip or by field-induced effects [20], leaving behind a perfectly stoichiometric area. However, the additional information accessible from the STM shows that a signature is retained where the original sOH resided. Single atom manipulation, induced by tip-surface interactions, is a well-known phenomenon, both laterally in the surface plane [9,21] and also perpendicular to the surface plane [22]. In this view, we tentatively interpret the transformation of the sOH species as a dynamic process where the on-top H of the surface OH is pushed to a subsurface site, forming a OH_{sub}. This situation would expose a stoichiometric topmost layer to the AFM tip, shielding the OH_{sub} and causing the surface region to appear perfectly stoichiometric. The formed subsurface OH_{sub} species, however, still perturb locally the electronic structure of the TiO_2(110) surface, rendering it

detectable in the STM. The fact that the Ti(5c) and the sOH show almost equal contrast with nc-AFM indicates, according to our previous results [10], that the surface was probed at a very short tip-surface distance, further rendering an atomic manipulation process probable.

The imaging of the sOH and OH_{sub} is illustrated in qualitative detail in the twin cross sections of Fig. 1(e) and the enlarged images in Figs. 2(a)–2(d), respectively. In Fig. 1(e), the AFM (Z) and STM (I_t) signals overlap, and it is observed that the normal 70 pm corrugation between Ti and O rows is continued on the OH_{sub} site—i.e., the surface topography appears completely unperturbed. In the STM (I_t) cross sections, on the other hand, a clear signature at the defect site both before and after with a tunneling current of 2.7 pA is observed in both graphs but with an additional ~0.2 pA dip displaced slightly away from the center of the O row. This asymmetry associated with the subsurface site is also apparent in the enlarged image in Fig. 2(d), where the protrusion is shifted towards one of the Ti rows.

To complement the interpretation of the experiment, we have investigated possible sites of H in TiO_2 and computed the energy barriers involved in the transfer of H between selected surface and subsurface sites. In the subsurface region, H preferentially bonds to O leading to the formation of a OH_{sub} at site 3 in Fig. 3(d). The reaction pathway illustrated in Fig. 3(a) further shows that sOH is ~0.4 eV more stable than OH_{sub}. However, the energy barrier for the H_{sub} to jump back to the surface and form a bridging sOH is ~2 eV, which is sufficiently high to block spontaneous backdiffusion of H at room temperature. Additionally, the rotation of H around the OH_{sub} site involves a ~0.7 eV energy barrier, and the migration between adjacent subsurface O(2c) rows has an energy barrier of ~1.9 eV [see Figs. 3(b) and 3(c)]. The theoretical results confirm that OH_{sub} is indeed stable at room temperature and H diffusion or OH_{sub} rotation is unlikely—i.e., the consistent asymmetric pattern in I_t images for OH_{sub} reflects that H is "frozen" in the specific subsurface location at site 3 in Fig. 3(d). The initial energy required to push the sOH hydrogen over the 2 eV barrier to the subsurface site is of the same order as in previous manipulation studies [21,23] and is much less than the >10 keV of the combined tip-cantilever system. Note also that, at higher H densities, the diffusion barrier into the surface may be reduced [24]. A comparison of the lateral positions in Figs. 2(b) and 2(d) before and after downwards diffusion of the H reveals that the OH_{sub} seems to have moved one lattice constant along the [001] row direction. Row diffusion has many similarities with surface diffusion of sOH, which has been found theoretically to have a high diffusion barrier of 1.5 eV [25,26]. We therefore attribute this jump to be a result of the manipulation process.

The connection between the H_{sub} site and its appearance as an electronic perturbation in the STM image is fully confirmed by STM simulations. We stress that the computed I_t images in this study take into account the detailed atomic structure of the tip. In Fig. 4, we display the simulated I_t of TiO_2(110) with surface OH and OH_{sub} using a Si(001)-Ti_3O_5 O-terminated tip. This tip model was pinpointed from our previous work [8]. In Fig. 4(a), the on-top H position (blue cross) induces the symmetric bright protrusion in between the Ti(5c) rows [see cross section in Fig. 4(c)]. The simulation of I_t for OH_{sub} predicts a remaining I_t between bright Ti(5c) rows as depicted in Fig. 4(b). This feature is more evident in the corresponding

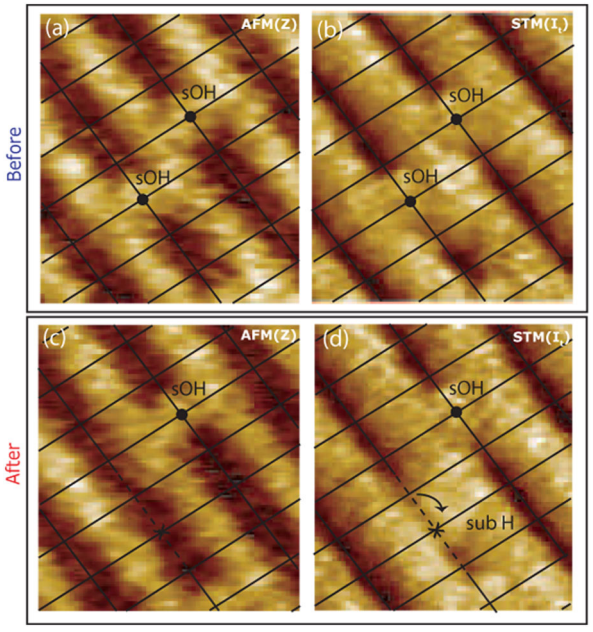

FIG. 2 (color online). (a),(c) Enlarged AFM (Z) images illustrating the surface before and after conversion of a sOH to a OH_{sub}. (b),(d) The corresponding enlarged STM (I_t) images. The superimposed grid illustrates the position of the bridging oxygen sublattice of TiO_2(110).

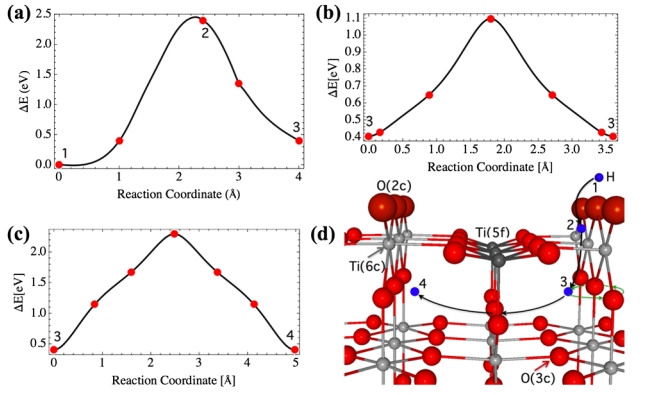

FIG. 3 (color online). (a)–(c) LDA + U minimum energy path calculations showing the energy diagram for (a) the sOH hydrogen to move to subsurface site 3, (b) H rotation around a O(3c) site, and (c) H diffusion from site 3 to 4. (d) Ball model of the TiO_2(110) surface where we sketch the hydrogen path between the marked sites.

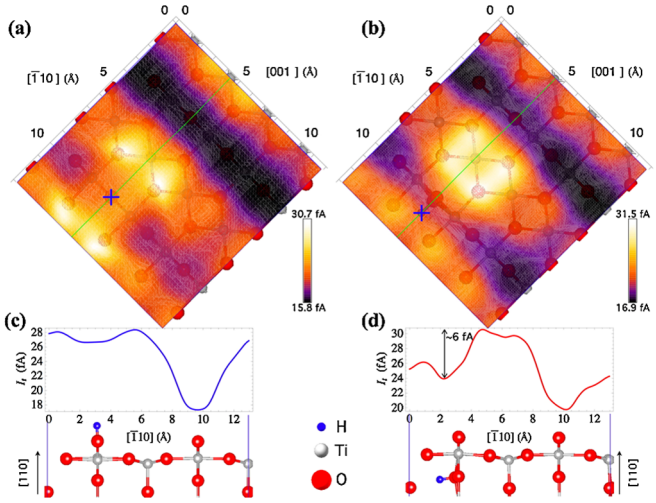

FIG. 4 (color online). Simulated I_t images with $U_{\text{bias}} = 0.5$ V for $TiO_2(110)$ with surface OH (a) and OH_{sub} (b). The $TiO_2(110)$ lattice is displayed beneath each image where the position of H is indicated by a blue cross. (c),(d) I_t shows cross sections along the green line from (a) and (b) together with a side view of the structure. O: red, Ti: blue, and H: gray.

cross section [Fig. 4(d)], where I_t shows a ~6 fA depression just above the OH_{sub} site in qualitative agreement with the experiment [Fig. 1(e)]. As in the experiment, there is an asymmetric local enhancement of I_t along the Ti(5c) trough adjacent to the H_{sub} [cf. Figs. 2(d) and 4(b)], emphasizing the electronic character of the features seen in STM due to the subsurface OH. The mismatch between the calculated and experimental I_t values was systematically investigated and could be accounted for by the influence of oxygen vacancies and Ti interstitials in the sample, tip-surface relaxations, and the limited size of tip [16].

In conclusion, we reveal that H atoms may exist at a stable interstitial site in rutile TiO_2 as a subsurface OH. The information on H_{sub} atoms was revealed from the combined complementary information in simultaneously recorded atom-resolved nc-AFM topography (Z) and tunneling current (I_t) signals and *ab initio* STM simulations which take into account the detailed tip structure. The simultaneous STM-AFM imaging method is generally applicable for analysis of defects in the subsurface region of conductors and semiconductors. As the combined STM-AFM method relies on active distance control by measuring forces only, it may enable new atom-resolved studies of materials with a very low conductivity, which are typically problematic for stable STM imaging. The method may therefore be ideally suited for analysis of subsurface H atoms or O vacancies in metal oxides such as CeO_2, ZnO, or anatase TiO_2, materials that have very wide technological applications.

S. Wendt is acknowledged for enlightening discussions. A. S. F. and H. P. P. acknowledge support from the Academy of Finland and generous grants of computing time from the Center for the Scientific Computing (CSC), in Espoo, Finland. The iNANO group acknowledges generous support from Haldor Topsøe A/S and Lundbeck Foundation as well as the Danish Research Council.

*adam.foster@tut.fi
†fbe@inano.dk

[1] H. S. Taylor, Proc. R. Soc. A **108**, 105 (1925).
[2] M. V. Ganduglia-Pirovano, J. L. F. Da Silva, and J. Sauer, Phys. Rev. Lett. **102**, 026101 (2009).
[3] A. Trovarelli, Catal. Rev. Sci. Eng. **38**, 439 (1996).
[4] S. Wendt *et al.*, Science **320**, 1755 (2008).
[5] C. G. Van de Walle and J. Neugebauer, Nature (London) **423**, 626 (2003).
[6] K. Xiong, J. Robertson, and S. J. Clark, J. Appl. Phys. **102**, 083710 (2007).
[7] H. Ö. Özer, S. J. O'Brien, and J. B. Pethica, Appl. Phys. Lett. **90**, 133110 (2007).
[8] G. H. Enevoldsen, H. P. Pinto, A. S. Foster, M. C. R. Jensen, A. Kuhnle, M. Reichling, W. A. Hofer, J. V. Lauritsen, and F. Besenbacher, Phys. Rev. B **78**, 045416 (2008).
[9] M. Ternes, C. P. Lutz, C. F. Hirjibehedin, F. J. Giessbl, and A. J. Heinrich, Science **319**, 1066 (2008).
[10] G. H. Enevoldsen, A. S. Foster, M. C. Christensen, J. V. Lauritsen, and F. Besenbacher, Phys. Rev. B **76**, 205415 (2007).
[11] U. Diebold, Surf. Sci. Rep. **48**, 53 (2003).
[12] F. J. Giessibl, Rev. Mod. Phys. **75**, 949 (2003).
[13] G. Kresse and J. Furthmüller, Comput. Mater. Sci. **6**, 15 (1996).
[14] G. Kresse and D. Joubert, Phys. Rev. B **59**, 1758 (1999).
[15] S. L. Dudarev, G. A. Botton, S. Y. Savrasov, C. J. Humphreys, and A. P. Sutton, Phys. Rev. B **57**, 1505 (1998).
[16] H. P. Pinto, G. H. Enevoldsen, J. V. Lauritsen, A. S. Foster, and F. Besenbacher (to be published).
[17] S. Kuck, H. Werheit, and O. Madelung, *Non-Tetrahedrally Bonded Binary Compounds* (Springer-Verlag, Berlin, 2000), 1st ed.
[18] G. Henkelman and H. Jónsson, J. Chem. Phys. **113**, 9978 (2000).
[19] K. Palotás and W. A. Hofer, J. Phys. Condens. Matter **17**, 2705 (2005).
[20] O. Bikondoa, C. Pang, R. Ithnin, C. Muryn, H. Onishi, and G. Thornton, Nature Mater. **5**, 189 (2006).
[21] Y. Sugimoto, M. Abe, S. Hirayama, N. Oyabu, O. Custance, and S. Morita, Nature Mater. **4**, 156 (2005).
[22] N. Oyabu, O. Custance, I. Yi, Y. Sugawara, and S. Morita, Phys. Rev. Lett. **90**, 176102 (2003).
[23] T. Trevethan, M. Watkins, L. N. Kantorovich, and A. L. Shluger, Phys. Rev. Lett. **98**, 028101 (2007).
[24] X.-L. Yin, M. Calatayud, H. Qiu, Y. Wang, A. Birkner, C. Minot, and C. Wöll, Chem. Phys. Chem. **9**, 253 (2008).
[25] S. Wendt, J. Matthiesen, R. Schaub, E. K. Vestergaard, E. Lægsgaard, F. Besenbacher, and B. Hammer, Phys. Rev. Lett. **96**, 066107 (2006).
[26] Z. Zhang, O. Bondarchuk, B. Kay, J. White, and Z. Dohnalek, J. Phys. Chem. B **110**, 21 840 (2006).